Mid-latitude ozone depletion and air quality impacts from industrial halogen emissions in the Great Salt Lake Basin

Caroline C. Womack[1,2], Wyndom S. Chace[3†], Siyuan Wang[1,2], Munkhbayar Baasandorj[4], Dorothy L. Fibiger[1,2‡], Alessandro Franchin[1,2#], Lexie Goldberger[5§], Colin Harkins[1,2], Duseong S. Jo[6], Ben H. Lee[5], John C. Lin[4], Brian C. McDonald[2], Erin E. McDuffie[1¶], Ann M. Middlebrook[2], Alexander Moravek[7||], Jennifer G. Murphy[7], J. Andrew Neuman[1,2], Joel A. Thornton[5], Patrick R. Veres[2], Steven S. Brown[2,8]*

1) Cooperative Institute for Research in Environmental Sciences, University of Colorado, Boulder, CO 80309
2) NOAA Chemical Sciences Laboratory, Boulder, CO 80305
3) Department of Chemistry, Williams College, Williamstown, MA 01267
4) Department of Atmospheric Sciences, University of Utah, UT 84112
5) Department of Atmospheric Science, University of Washington, Seattle, WA 98195
6) Atmospheric Chemistry Observations and Modeling Laboratory, NCAR, Boulder, CO 80307
7) Department of Chemistry, University of Toronto, ON, M5S 1A1, Canada
8) Department of Chemistry, University of Colorado, Boulder, CO 80309

KEYWORDS: Halogens; Oxidants; Air quality; Industrial emissions; Chemical modeling

ABSTRACT: We report aircraft observations of extreme levels of HCl and the dihalogens Cl_2, Br_2, and BrCl in an industrial plume near the Great Salt Lake, Utah. Complete depletion of O_3 was observed concurrently with halogen enhancements as a direct result of photochemically produced halogen radicals. Observed fluxes for Cl_2, HCl, and NO_x agreed with facility-reported emissions inventories. Bromine emissions are not required to be reported in the inventory, but are estimated as 173 Mg year^{-1} Br_2 and 949 Mg year^{-1} BrCl, representing a major uncounted oxidant source. A zero-dimensional photochemical box model reproduced the observed O_3 depletions and demonstrated that bromine radical cycling was principally responsible for the rapid O_3 depletion. Inclusion of observed halogen emissions in both the box model and a 3D chemical model showed significant increases in oxidants and particulate matter ($PM_{2.5}$) in the populated regions of the Great Salt Lake Basin, where winter $PM_{2.5}$ is among the most severe air quality issues in the U.S. The model shows regional $PM_{2.5}$ increases of 10 – 25% attributable to this single industrial halogen source, demonstrating the impact of underreported industrial bromine emissions on oxidation sources and air quality within a major urban area of the western US.

SYNOPSIS STATEMENT: High industrial halogen emissions may be contributing significantly to poor wintertime air quality in Utah's Great Salt Lake Basin.

TOC GRAPHIC:

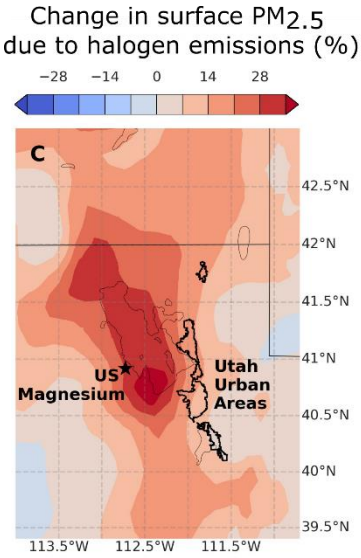

39

40

41 MAIN TEXT:

42 I. Introduction

43 Halogens are atmospheric oxidants that affect ozone (O_3) concentrations and the oxidative
44 capacity of the troposphere[1, 2]. Halogen-induced ozone depletion events have often been observed
45 in the stratosphere and in tropospheric polar regions in springtime[3, 4]. The simplified mechanism
46 for bromine-induced depletion in the polar troposphere is[1]:

47 $HOBr(aq) + Br^-(aq) \rightarrow Br_2(g) + OH^-(aq)$ (R1)

48 $Br_2 + hv \rightarrow 2Br\cdot$ (R2)

49 $Br\cdot + O_3 \rightarrow BrO + O_2$ (R3)

50 $BrO + BrO \rightarrow Br_2$ or $2Br\cdot + O_2$ (R4)

51 $BrO + HO_2 \rightarrow HOBr + O_2$ (R5)

52 with a similar mechanism for chlorine and iodine radicals. Reactions (R1) – (R5) represent a
53 catalytic net O_3 destruction cycle, starting with aqueous-phase generation of dihalogens[1]. In the
54 absence of high levels of nitrogen oxides (NO_x) or volatile organic compounds (VOCs) that quench

55 the cycle, such as in the remote Arctic, small quantities of Br, Cl, or I radicals can be responsible
56 for significant levels of O_3 depletion[4].

57 Atmospheric chlorine and bromine have also been observed in the midlatitude marine
58 boundary layer and over continental salt lakes and attributed to conversion of natural sources such
59 as sea salt or marine organohalogens to more reactive forms[1], and where reaction with NO_x and
60 VOCs plays a more substantial role, as in the following simplified mechanism

61 $$XO + NO_2 \rightarrow XONO_2 \quad \text{(R6)}$$

62 $$XONO_2 + H_2O\ (aq) \rightarrow HOX \text{ or } X_2 + HNO_3 \quad \text{(R7)}$$

63 $$X + VOC \rightarrow\rightarrow RO_2 + HX \quad \text{(R8)}$$

64 where X represents a halogen atom. One prevalent mechanism in the midlatitudes is the conversion
65 of N_2O_5 to $ClNO_2$ on the surface of chloride-containing aerosol[5-7]. Transport of halogen reservoirs
66 such as $ClNO_2$, which may also be formed by the reaction of Cl radicals with NO_2, has implications
67 for the downwind oxidizing capacity of the troposphere[1, 8], and several recent studies have
68 demonstrated the impact of gas-phase halogen species on urban air quality[9-11] via reaction with
69 NO_x and VOCs. Halogens also convert elemental mercury to oxidized mercury[12, 13], and dimethyl
70 sulfide to sulfate[14]. However, a complete understanding of these mechanisms is still limited due to
71 insufficient observations.

72 High levels of bromine monoxide (BrO) have been observed both in situ and via satellite
73 near continental salt lakes and salt marshes[15-21], and have been attributed to the reaction of Br
74 radicals with O_3 (R3). The Dead Sea is one of the saltiest bodies of water on Earth at approximately
75 340 g/kg[22], and numerous studies have shown high levels of BrO and O_3 depletion events in its
76 vicinity[15-18]. Through observations with a long path differential optical absorption spectroscopy
77 (LP-DOAS) instrument, and supported by observations from the OMI satellite instrument,

concentrations of up to 200 parts per trillion (ppt) of BrO have been observed throughout the year[16, 17], and largely attributed to natural lake sources. Other salt lakes across the world[19, 20], including the Great Salt Lake in the US[21] have displayed similar behaviors, albeit at lower levels. The Great Salt Lake salinity varies depending on water level and is higher in the northern half, but typically ranges from 140 – 320 g/kg[23].

In 2002, Stutz *et al*. observed BrO and ClO concentrations of up to 6 ppt and 15 ppt, respectively, at a site on the southeast shore of the Great Salt Lake[21]. Using back trajectory calculations, they also attributed these observations to natural sources, and ruled out contributions from an industrial magnesium refinery on the west side (US Magnesium, known before 2002 as MagCorp). US Magnesium isolates $MgCl_2$ salt from pre-concentrated lake salt brine and electrolyzes the salt to generate magnesium, with chlorine gas as a known byproduct. Over the past several decades, US Magnesium has reported significant reductions in its molecular chlorine (Cl_2) and hydrochloric acid (HCl) emissions, but between 2010 and 2020, its Cl_2 emissions still represented between 50 and 85% of the total yearly US industrial point source chlorine emissions inventory[24], and 2017 was the highest emission year in that decade. Molecular bromine (Br_2) and bromine chloride (BrCl) are not in the US Environmental Protection Agency's list of Hazardous Air Pollutants (HAPs), and the national emission inventories therefore do not provide estimates of those species.

In this paper, we report on observations made during the 2017 Utah Winter Fine Particulate Study (UWFPS), an aircraft- and ground-based field intensive based in Salt Lake City that studied the build-up of ammonium nitrate aerosol pollution during wintertime stagnant air episodes[25]. The instrumented NOAA Twin Otter aircraft, which included an iodide chemical ionization mass spectrometer (I^- CIMS) for bromine- and chlorine-containing species detection and a cavity

ringdown spectrometer (CRDS) for NO_x and O_3 detection, repeatedly sampled atmospheric emissions from the US Magnesium plant over the Great Salt Lake. We observed extreme levels of Br_2, Cl_2, BrCl, and HCl in these plumes, associated with widespread O_3 depletions in the daytime as the air mass was transported across the lake towards the Salt Lake City urban area. We use nighttime observations to estimate the emissions fluxes of Cl_2, Br_2, BrCl, HCl and NO_x from the plant. We then use a zero-dimensional photochemical box model to reproduce the observed halogen-induced O_3 depletions in the plumes during daytime transects and a 3D chemical model to estimate the effect of these emissions on winter $PM_{2.5}$, a longstanding air quality issue, within the broader Great Salt Lake Basin. These emissions provide an opportunity to test current understanding of otherwise uncertain halogen chemistry and chemical mechanisms from a well-defined emission source and transport pattern.

II. Methods

a. The Utah Winter Fine Particulate Study

The Utah Winter Fine Particulate Study (UWFPS) was a 4-week ground- and aircraft-based field intensive that has been described extensively[25-30]. Gas phase species were measured on the NOAA Twin Otter aircraft at a 1 Hz time resolution. The halogen species Cl_2, Br_2, BrCl, HCl, HOCl, HOBr, $ClNO_2$, and $BrNO_2$, and the inorganic nitrogen species N_2O_5, HNO_3, and HONO were detected with the University of Washington iodide adduct chemical ionization mass spectrometer (I- CIMS)[31, 32]. Calibration factors for HOBr and $BrNO_2$ were estimated using quantum chemical calculations[33], and for all other species using calibration sources before, during, and after the campaign, as in Lee *et al*[32]. Zeros were conducted every 30 seconds in flight using overflowed zero air. Elevated levels of signal were detected at the m/z ratios corresponding to ClO

and BrO but in the absence of a reliable calibration, were not used in this analysis. Likewise, masses attributed to iodine-containing species could not be adequately differentiated from those resulting from reagent chemistry inside the instrument, and were therefore could not be used here. The NOAA Nitrogen Oxide Cavity Ringdown Spectroscopy (NOxCaRD) instrument reported NO, NO_2, O_3, and NO_y[34]. A customized Aerosol Mass Spectrometer (AMS) measured the mass of non-refractory submicron aerosol (PM1) at 0.1 Hz, as well as its chemical composition of NH_4^+, NO_3^-, Cl^-, SO_4^{2-}, and organic aerosol[35, 36]. An Ultrahigh Sensitivity Aerosol Spectrometer (UHSAS) measured the dry aerosol size distributions between 70 and 1000 nm diameter[37] and corresponding aerosol surface area, and no correction was made in this analysis to account for water uptake to aerosol. A commercial meteorological probe (Avantech) measured wind direction and speed, pressure, temperature, relative humidity, and the aircraft GPS position and altitude. Table S1 summarizes the instrument accuracy and lower detection limits during UWFPS.

b. Deriving plume ages with the STILT model

Plume transects were identified based on concentrations above the ~0.3 ppt detection limit of one or more of the primary halogens (Cl_2, Br_2, and BrCl). Further evidence of the US Magnesium plant influence was provided by back trajectory calculations linking the sampled plumes to emissions from the facility. The Stochastic Time-Inverted Lagrangian Transport (STILT) model[38] was used to calculate the back trajectories for air parcels along the Twin Otter flight tracks, and to approximate plume ages. STILT is a Lagrangian particle transport model that uses gridded meteorological fields from the NOAA High-Resolution Rapid Refresh model[39] to follow an ensemble of 200 "particles", representing air parcels, back in time from a given receptor point. During the UWFPS field intensive, the STILT model was run every 1 – 2 minutes along each Twin Otter flight track[29], totaling approximately 2,500 individual model runs. A STILT

147 particle was considered to have passed the US Magnesium plant if it came within 40% of the
148 distance between the plant and the receptor point. This value was empirically chosen to best filter
149 trajectories into those that passed by the plant. Ages were calculated as the trajectory time between
150 the receptor and the point of closest approach to the facility.

151 To determine the plume age of a given observed plume, we averaged the age of the nearest
152 STILT trajectory receptor points. If no appropriately nearby trajectories were available, we
153 calculated the instantaneous wind speed from the nearest STILT trajectories and converted to
154 plume age using the distance of the aircraft from the plant stack. This assumes a straight-line
155 trajectory and was only used for observations very close to the plant, where the aircraft performed
156 tight spirals and the nearby trajectory calculations were not sufficiently precise to estimate the
157 plume age.

158 To estimate the emission fluxes of Cl_2, Br_2, BrCl, HCl, and NO_x from the US Magnesium
159 plant, we used three nighttime flights (February 8, 11, and 12) where emissions were diluted during
160 transport and unaffected by photochemistry. Of the 13 plume transects encountered on those three
161 flights, we selected six that passed most perpendicularly to the wind direction and through the
162 central portion of the plume. NO_x and halogens peaks were not always coincident in space near
163 the plant, indicating separate emission stacks for the chemical waste and the power plant waste.
164 Using a typical flux measurement strategy[40-42], we assumed a spherical plume, integrated the data
165 across the cross-sectional transect, and multiplied by the horizontal wind speed (Figure S1) to yield
166 average emission fluxes.

167 c. F0AM box modeling

168 To understand the observed O_3 depletions, we constructed a photochemical box model
169 using the Framework for 0-dimensional Atmospheric Modeling (F0AM v4.2)[43], driven by a subset

of the Master Chemical Mechanism v3.3.1[44] that included all the inorganic chemistry, as well as the reactions of the set of measured VOCs (see below). The F0AM model does not explicitly consider aerosol microphysics, so for simplicity, total nitrate (HNO_3 + pNO_3^-) and total chloride (HCl + pCl^-) were treated here without consideration of gas-particle partitioning.

To model the halogen chemistry, we followed Sherwen *et al*[45], Thompson *et al*[4] and others[46, 47] in constructing a mechanism based on the reactions in the compiled recommendations[48-51] or other literature[8, 52-56]. This mechanism, which rectifies several typographical errors in the appendices of Sherwen *et al*[45], included interactions of Br and Cl radicals with O_3, OH, NO_x, and all other inorganic species, as well as with small organic molecules including aldehydes, ketones, aromatics, alkanes, alkenes, alkynes, and organic acids. Most of these halogen-VOC reactions occur via a hydrogen abstraction to form HBr or HCl plus a peroxy radical, whose subsequent chemistry is already in the MCM mechanism. However, the reaction of Cl and Br radicals with the unsaturated bonds in small alkenes occurs via an addition across the double bond, resulting in a halogenated hydrocarbon peroxy radical. Following Xue *et al*[52] and Riedel *et al*[8], we explicitly account for these subsequent reactions of the products of Br and Cl radicals with C_2H_4 and C_3H_6. The full halogen mechanism is shown in Tables S2 – S4 and Figures S2 – S5. The entire mechanism contains 1500 species and 4600 reactions.

Measured plume transects represented air masses that had been emitted anywhere from 10 minutes to many hours earlier but the aircraft sampling strategy was non-Lagrangian. We therefore uesd a "puff" style model[57], in which a parallel submodel was run for each observed transect. Each submodel ran under identical parameters, but was initialized at the estimated time of day of emission and run through the full lifetime of each transect. The final concentration of each

192 submodel was used to construct the modeled output, which was then compared with the
193 observations.

194 The puff model was initialized with concentrations for Cl_2, Br_2, HCl, BrCl, and NO, scaled
195 to match the daytime plume observations of each transect. A first order dilution constant was scaled
196 to fit the observed recovery of the O_3 depletion over time. Following our previous work, an average
197 profile of VOC concentrations was constructed for each modeled day based on the VOCs measured
198 by the University of Minnesota Proton Transfer Reaction Mass Spectrometer (PTR-MS) at the
199 University of Utah ground site on the northeast side of the Salt Lake Valley during UWFPS[30].
200 Other VOCs were scaled with a previously determined scaling factor[30, 58]. An additional scaling
201 factor of 0.5 was applied to the profile to account for lower VOC concentrations over the Great
202 Salt Lake and further from the urban center, derived empirically from the average ratio of aircraft
203 $PM_{2.5}$ total concentrations over the Salt Lake Valley and over the Great Salt Lake during pollution
204 episodes. Further model details can be found in section S1.

205 Once optimal parameters were obtained for the puff model, a single averaged model was
206 run with average model parameters, an average value for Cl_2, and all other species scaled to Cl_2
207 with to the molar ratios determined in the emissions analysis (see section III.a) to investigate
208 reaction rates and Br and Cl radical chain lengths. This averaged model was initialized at 9am on
209 a typical wintertime polluted day and was allowed to run for 6 hours, which is approximately the
210 time needed to travel the 40 km across the lake with a 2 m/s wind speed. It was run with and
211 without the halogens to determine their control over oxidants.

212 Sensitivity tests were conducted to investigate whether any model assumptions
213 significantly affected the model predictions. The "average" model was run with the following
214 parameters scaled up and down by 20%: NO_x and VOC concentration, aerosol surface area,

photolysis rates, and the dilution constant. Additional tests adjusted the N_2O_5 uptake parameter, whether or not bromine chemistry was included, and whether a high amount of NO_x was initially emitted from the US Magnesium stack.

d. CAM-chem 3-D modeling

The CAM-chem model[59] with regional refinement (part of the Community Earth System Model, version 2.2)[60] is used in this work, which is part of the Multiscale Infrastructure for Chemistry and Aerosols (MUSICA) version 0[61, 62]. Temperature and winds are nudged toward the MERRA2 meteorology (Modern-Era Retrospective analysis for Research and Applications, version 2)[63], with 32 vertical layers (surface to ~3 hPa) and a horizontal resolution of ~14 km across over the continental U.S. and ~111 km across over the rest of the globe. The MOZART-TS1 mechanism is used in this work, including key chemical reactions in the troposphere and stratosphere[60]. Halogen chemistry has been elaborated previously by Wang *et al*[64] and references therein. Aerosols are calculated using the Modal Aerosol Model with four modes (MAM4)[65] coupled with the Model for Simulating Aerosol Interactions and Chemistry (MOSAIC)[66, 67], including sulfate, ammonium, nitrate, primary organic matter (POM), secondary organic aerosol, sea salt, and mineral dust.

The global monthly CAMS (Copernicus Atmosphere Monitoring Service) emission inventory are used for anthropogenic emissions globally[68], with the anthropogenic emissions over the continental U.S. replaced with regional-scale hourly emission inventories for mobile source and volatile chemical product emissions using FIVE-VCP (Fuel-based Inventory of Vehicle Emissions and Volatile Chemical Products)[69], oil and gas emissions using FOG (Fuel-based Oil and Gas inventory)[70], and other anthropogenic emissions from the NEI 2017[71]. Inorganic halogen

and NO_x emissions from US Magnesium were taken from this work. Other aspects of the model configuration are similar to those described in Fung *et al*[66]. Section S2 details the model validation.

III. Results and Discussion

a. Estimation of halogen emission fluxes from US Magnesium

Using the emissions flux method described in section II.b, we obtained average emissions fluxes of 90, 50, 6, 30, and 30 g/sec for Cl_2, HCl, Br_2, BrCl, and NO_x, respectively (Table 1). The wide range in observed fluxes are a result of plume heterogeneity and variability in instantaneous emissions, as well as the simplifying assumptions of plume shape.

Species	Observation-derived emission flux (full range) (g/sec)	Annual inventory-derived emission flux (g/sec)
Cl_2	90 (11 – 351)	114.17
HCl	50 (1 – 138)	30.50
Br_2	6 (0 – 20)	Not reported
BrCl	30 (4 – 111)	Not reported
NO_x	30 (1 – 103)	28.91

Table 1. *Calculated emission fluxes from six nighttime transects of the US Magnesium emission plume, compared with facility-reported inventory emission fluxes.*

Table 1 also shows the US Magnesium facility-reported mass of emissions from the US EPA 2017 Toxic Release Inventory (TRI) for Cl_2 and HCl[24], and the US EPA 2017 National Emissions Inventory (NEI) for NO_x[71]. The reported stack emissions of 3600.35 Mg of Cl_2, 961.70 Mg of HCl and 912.59 Mg of NO_x reported in 2017 are converted to 114.17 g/sec Cl_2, 30.50 g/sec HCl and 28.91 g/sec NO_x, assuming a constant emission rate throughout the year, in the absence of any further temporally resolved emissions estimates. We also assume minimal NO_x oxidation or uptake of halogens on aerosol in the <30 minutes between emission and sampling, based on their relatively slow rates on this time scale. Our average estimates are within a factor of two of the reported estimates, despite their wide range. The TRI does not report bromine emissions, but

converting the observation-derived fluxes in Table 1 yields estimated yearly emissions of 173.76 Mg year^{-1} of Br_2 and 948.91 Mg year^{-1} of BrCl. It is difficult to compare these numbers to other industrial emissions, as bromine is rarely reported, but these likely represent a major unreported oxidant source. There were other minor chlorine sources observed during the campaign, but none that emitted any detectable bromine (Figure S6).

During the three selected nighttime flights, the closest aircraft-plume transects were estimated to be 1-2 minutes downwind of the plant stack. The largest concentrations observed during these transects were 600 parts per billion (ppb) of Cl_2, 3 ppb of Br_2 and 100 ppb BrCl. To our knowledge, these are the highest levels of these halogens ever measured in ambient air[2], outside of Cl_2 in volcanic plumes[72]. Section S3 and Figures S7 – S8 discusses any potential interferences from these large halogen concentrations, but they are not expected to affect the following results.

b. Photochemical box modeling

A box model of daytime plume transects was used to investigate the impact of halogen emissions on O_3. During the UWFPS campaign, there were 67 individual plume transects measured over nine flights on seven separate days (16, 17, 18, 26, 27, 28, and 31 January 2017). The plumes all showed evidence of complete and rapid O_3 depletion in the first several minutes after emission. The spatial distribution of these transects is shown overlain on the Twin Otter flight tracks in Figure 1a, and the coloring in the left and right panels show the Br_2 concentrations and the extent of O_x depletion. O_x ($O_3 + NO_2$) is shown here to demonstrate that the O_3 depletion cannot be attributed to the rapid reaction of O_3 with NO, which would form NO_2 and therefore conserve O_x. A time series of halogens and O_x observations (Figure S9) during one of these flights highlights the anti-correlation between the halogens and O_x and the low concentrations of NO_x. During the

flight path across the Great Salt Lake, the Twin Otter encountered the O_3-depeleted plume confined within a discrete altitude range, confirming a lofted plume source isolated from the surface, rather than a natural lake source (Figure S10). Figure 1 demonstrates that emissions from US Magnesium are concentrated near the plant, but extend to nearly the entire Wasatch Mountain Front, as evidenced by partial O_3 depletions as far west as Salt Lake City, UT and as northwest as Ogden, UT, both approximately 60 km away.

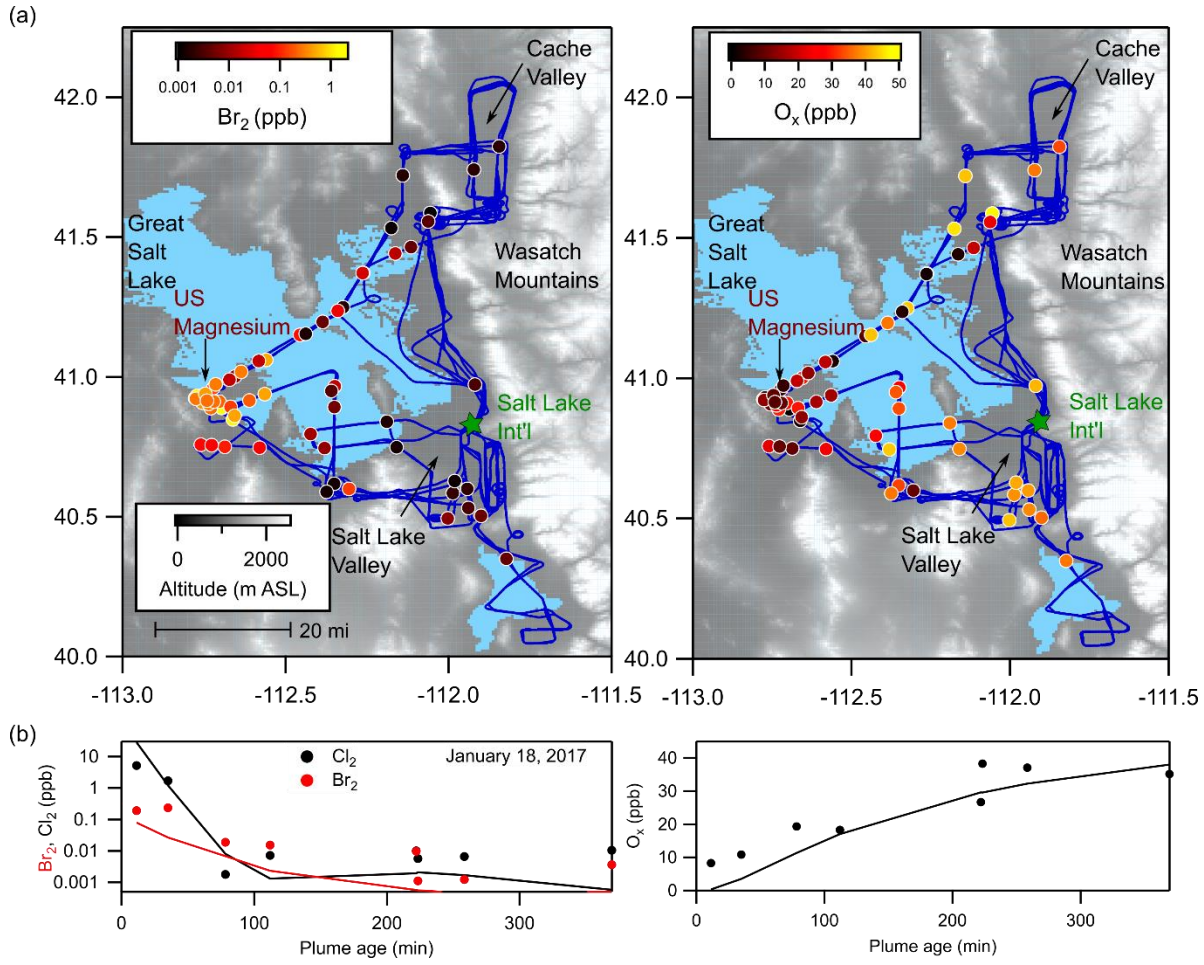

Figure 1 (a) Flight tracks of the NOAA Twin Otter aircraft (blue line) overlaid on a terrain area map, with individual plume transects throughout the campaign shown as colored markers with the color scale indicating Br2 concentration on the left, and O_x (O_3 + NO_2) on the right. The regional background O_x level was approximately 45 ppbv outside of urban or industrial influence. Wind

direction varied throughout the campaign, leading to plume detections all along the Wasatch Mountain Front. Transects from the January 18, 2017 plume are plotted against plume age in panel (b). Solid lines show the model output of the F0AM photochemical box model

The measured Br_2, Cl_2 and O_x concentrations in the January 18 mid-afternoon plume are shown in Figure 1b, demonstrating an initially high level of halogens near the plant that decreases due to photolysis and dilution within the first hour, as well as the immediate depletion of O_x. Because of the low wind speeds, the freshest plume transects were at least 7 to 10 minutes old. With typical halogen concentrations in the fresh plume, a Br_2 photolysis rate of 0.03 s^{-1}, and a O_3 + Br· rate constant of 8.3 x 10^{-13} cm^3 $molecule^{-1}$ s^{-1} [49], substantial O_3 depletion is estimated to occur within in the first few minutes after emission. The recovery of the O_3 concentration after the first hour, and the continued decrease of the halogens, is due to entrainment of low-halogen background air into the plume as it transports downwind.

Figure 1b shows the F0AM-modeled Br_2, Cl_2 and O_x for January 18 in solid line, which shows reasonable agreement with the observations. Model-observation correlations of the major species for all eight plumes (67 transects) are shown in Figure 2. Model parameters for each of the eight plumes, which were generally consistent, are shown in Table S5. Correlations for the minor species HONO, N_2O_5, HOBr, HOCl, $BrNO_2$ and $ClNO_2$ are shown in Figure S11.

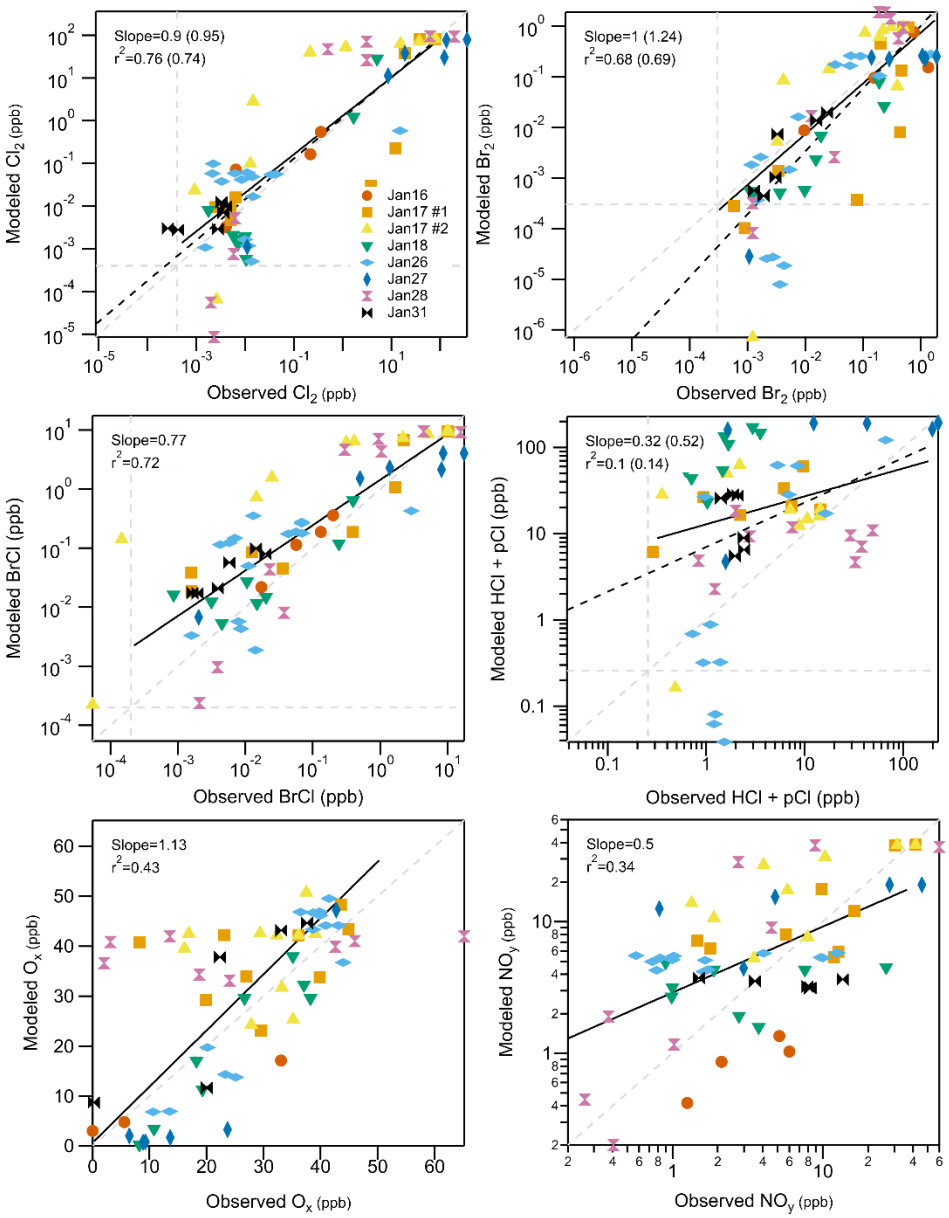

308

309 *Figure 2. Correlation plots of modeled (y-axis) vs observed (x-axis) concentrations for all eight*
310 *plumes (67 transects) and six key species: Cl_2, Br_2, BrCl, HCl + pCl^-, O_x, and NO_y. Dashed grey*
311 *lines show the 1:1 line and the limits of detection (LOD) for the observed species. The black lines*
312 *show two linear fits, one including all data (solid) and one including just data above the LOD*
313 *(dashed), with the slope and r^2 given in the top left of each plot. If the two fits yielded different*
314 *parameters, the values in parentheses give those from the fit to data above the LOD. The model*
315 *and observations agree well across a wide range of observations for most of the species.*

316 The data in Figure 2 generally fall along the 1:1 line and the correlation coefficients (r^2)
317 are generally above 0.4, with some exceptions, indicating reasonable agreement between the model
318 and observations, particularly given the simplicity of the model and the wide range of the observed
319 concentrations. The overall agreement is lower for HCl + pCl^- and for NO_y. Since the I- CIMS
320 sensitivity to HCl is approximately 100 times less than for dihalogens[32], the HCl measurement
321 imprecision is larger than for the other halogens (Table S1).The agreement is especially poor on
322 Jan 18, for reasons that could not be determined, and removing this one day from the fit increases
323 the slope and r^2 to 0.46 and 0.22, respectively. The lower agreement in NO_y is largely driven by
324 NO_x, and the difficulty in accounting for other nearby anthropogenic NO_x sources across the Great
325 Salt Lake Basin which could not be easily incorporated into the 0D model. Other model-
326 observation discrepancies occurred in HOBr and $BrNO_2$ (Figure S11), two species with poorly
327 quantified aerosol uptake coefficients[46]. However, we demonstrate in the sensitivity tests (section
328 II.c and Figure S12) that the results of the model are valid despite the discrepancies listed here.
329 The model was then used to investigate the chemical processes within the plume as it
330 travels towards the populated Salt Lake and Cache Valleys, as described in Methods. Figure 3
331 shows that the majority (~90%) of the net O_3 depletion is caused by reaction with Br atoms, with
332 O_3 + Cl· making up the remainder. Although the Br radical is less abundant than the Cl radical, its
333 reaction with O_3 is faster and consequently the Br radical dominates O_3 loss in the first minutes.
334 Additionally, Cl radicals are rapidly lost to VOCs, including methane, methanol, ethane, and
335 propane, whereas Br radicals react primarily with O_3. Once O_3 is depleted, the reactions of the Br
336 radical with formaldehyde (HCHO), acetaldehyde (CH_3CHO) and propylene (C_3H_6) dominates Br
337 radical loss.

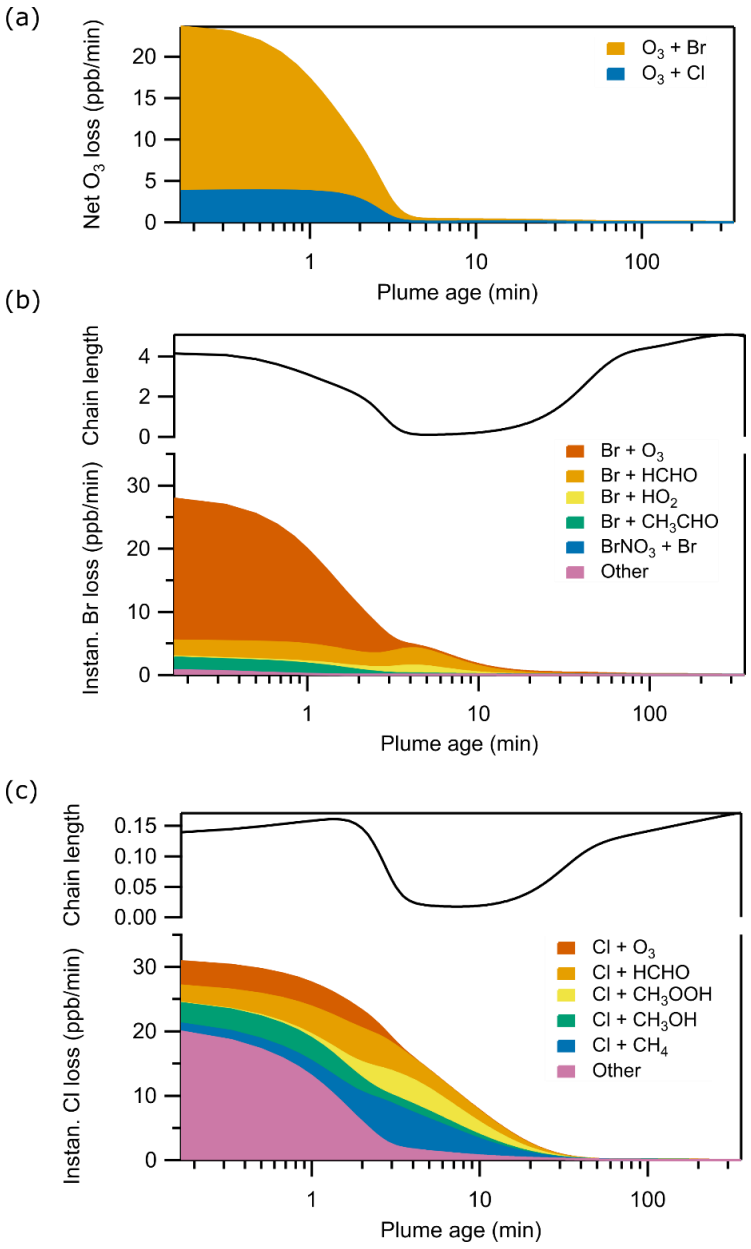

338

339 *Figure 3. The modeled top loss processes for O_3, Br· and Cl·. (a) The top net loss processes for O_3*

340 *are the reactions with Br·, followed by Cl·. Panels (b) and (c) show that O_3 depletion is the major*

341 *instantaneous loss process for Br radicals, and the dominant mechanism for Cl radicals is*

342 *reactions with VOCs such as methane and formaldehyde. The "other" category for Cl radical loss*

343 *contains 36 reactions and is dominated by reactions with small alkanes, alkenes, aldehydes, and*

peroxy radicals. The upper trace in panels (b) and (c) show the calculated chain length of Br and Cl radicals.

In the first 60 seconds of the simulation, O_3 depletion by the halogen radicals dominates the chemistry. In the first 60 minutes, reactions of Cl and Br radicals with VOCs dominate in the absence of O_3. After that, the entrainment of background air with approximately 42 ppb O_3 into the plume allows the O_3 + Br· or Cl· chemistry to restart. For the last 5 hours of the simulation, the Br and Cl radicals undergo reactions that balance between propagation of the ozone-depletion mechanism (R1) – (R5), and the termination via reaction with VOCs. Following Thompson *et al*[4], we quantify that branching by calculating the Br and Cl radical chain lengths as the ratio of cycle-propagation reactions (i.e. Br· + O_3 → BrO) to the termination reactions (i.e. Br· + VOCs → HBr + products). The calculated chain lengths are a metric of how effectively each radical depletes O_3, and are shown in the upper portion of Figures 3b and 3c. Both exhibit a minimum value when O_3 is depleted, and termination reactions dominate, and increase in the latter part of the simulation. The bromine chain length is ~20 times higher than the chlorine chain length, because Br radicals more readily regenerate Br_2 and BrCl to restart the ozone-depletion process, while Cl radicals mostly terminate with VOCs. The values found here are close to those recently determined in the tropospheric Arctic[4] but much smaller than those in the stratosphere[3] where VOC mixing ratios are much smaller.

c. Effects on air quality

The Salt Lake Valley regularly experiences $PM_{2.5}$ pollution episodes in the wintertime that are dominated by ammonium nitrate aerosol, which is formed from gas phase reaction between ammonia (NH_3) and nitric acid (HNO_3)[26, 73, 74], and ammonia tends to be in excess[27]. Previous modeling[30] demonstrated that the formation of HNO_3, which comes from the reaction of NO_x and

VOCs, is most sensitive to reductions in VOCs, due to their role in producing HO_2 and RO_2 radicals, which convert NO to NO_2 without the loss of O_3. NO_2 can then undergo daytime (NO_2 + OH) or nighttime (N_2O_5 uptake) processing to form HNO_3 which readily forms ammonium nitrate aerosol[30]. We therefore use two complementary methods to estimate the effect of halogens on $PM_{2.5}$ formation. In the first, we evaluate the chemical evolution within a typical plume constrained to observations using the box model described in section II.c. In the second, we use a 3D chemical model to estimate the $PM_{2.5}$ formation across the Great Salt Lake basin.

Figure 4a shows two box model runs, one with the average US Magnesium halogen emissions derived from nighttime transects, and one without. We examine the concentrations of several key species, RO_2, HO_2, and $HNO_3 + pNO_3^-$, at the end of the box model. The enhancement for each species is calculated as the percentage increase in concentration between the halogens model and the non-halogens model after six hours of processing. The presence of halogens is associated with a 32% increase in predicted HO_2, a 54% increase in RO_2, and a 106% increase in $HNO_3 + pNO_3^-$ in the plume. These increases are of critical importance, as they all play a role in the build-up of ammonium nitrate aerosol.

To determine whether the simplifying model assumptions affect the conclusions, sensitivity tests were conducted. The resulting enhancements of HO_2, RO_2, and $HNO_3 + pNO_3^-$ are shown in Figure S13, and confirm that halogens still increase the production of oxidants in all modeled cases. The only exception is the sensitivity test in which bromine chemistry is not included. In that case, HO_2, and RO_2 are only marginally enhanced by the presence of chlorine only, but $HNO_3 + pNO_3^-$ is not enhanced at all. This indicates that bromine is playing a key role in these enhancements.

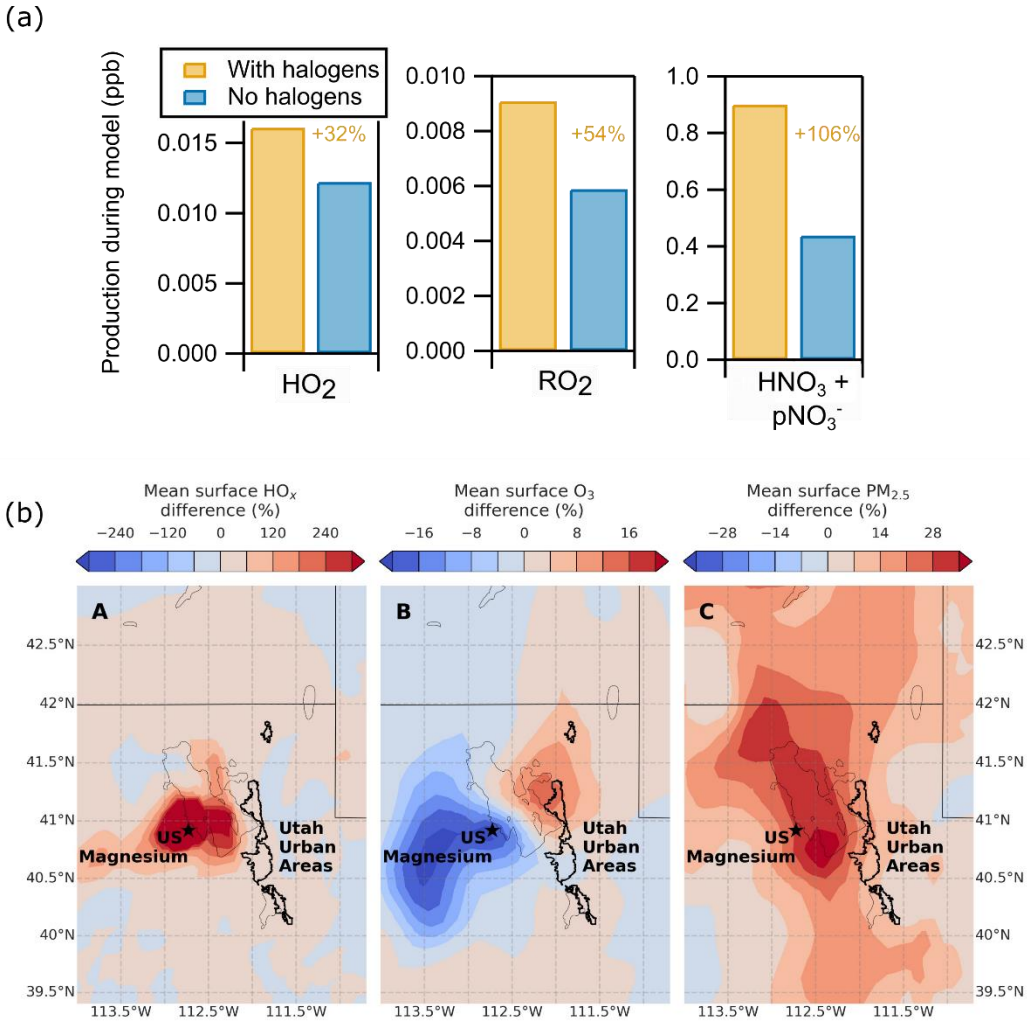

Figure 4(a) The modeled concentrations of three key species at the end of the 6-hour 0D photochemical box model run with halogens (yellow bars) and without halogens (blue bars). HO_2, RO_2, and $HNO_3 + pNO_3^-$ are enhanced in the plume by 32%, 54%, and 106% respectively by the presence of halogen emissions. (b) The change in surface HO_x, O_3, and $PM_{2.5}$ during a February 2017 pollution episode when US Magnesium halogen emissions are included, as estimated by the CAM-chem model The $PM_{2.5}$ increase was found to be driven by the increase in ammonium nitrate.

We then used the global CAM-chem 3D model with regional refinement[60] of 14 km spatial resolution over Utah. The model was run with and without the halogen emissions for the month of February 2017 to estimate the formation and destruction of pollutants by the halogens. The model tended to underpredict total $PM_{2.5}$ somewhat due to known difficulties modeling the shallow boundary layer, but differencing the halogens and non-halogens model runs largely mitigates this issue by calculating relative changes. Section S2 details the model validation. Figure 4b shows the estimated change in HO_x, O_3, and $PM_{2.5}$ in the Great Salt Lake basin during one pollution episode measured during the UWFPS campaign. HO_x is greatly enhanced in the immediate vicinity of the US Magnesium plant, while $PM_{2.5}$ is increased throughout the basin, with the populated areas on the south and southeastern parts of the Salt Lake showing a 10 – 25% increase in $PM_{2.5}$. This increase is principally due to increases in ammonium nitrate aerosol (Figure S18). O_3 demonstrates a different pattern, with depletions near the plant due to reactions with halogen, and increases of up to 10% further downwind from the plant due to the enhanced production of HO_2. Figure S19 shows an analogous model with bromine emissions only, demonstrating that bromine dominates the O_3 depletion, but both chlorine and bromine emissions contribute to the increase in $PM_{2.5}$.

The two models together represent the full chemical complexity in this system. The 0D box model shows the detailed chemistry occurring within the plume, and is tightly constrained to observations. Meanwhile, the 3D chemical model can examine the widespread effects of the emissions over a multi-day period. Counties in the Great Salt Lake basin regularly experience exceedances of the National Ambient Air Quality Standard (NAAQS) of 35 $\mu g\ m^{-3}$ during these pollution episodes. Both models described here indicate enhanced particulate nitrate resulting from oxidation by halogens, and strongly point to their role in negatively affecting air quality in the region.

d. Other impacts of halogen emissions

We note three possible additional implications of environmental impacts from industrial halogen emissions that may be addressed in further measurements in the region. The first is that Br radicals react readily with gaseous elemental mercury (Hg^0) to form gaseous oxidized mercury (Hg^{II})[12, 13, 75], which then is taken up into the condensed phase and enters the aquatic water system as a toxin. Mercury is monitored by the Atmospheric Mercury Network[76] and the two sites in the Great Salt Lake area are noted for their relatively high levels of Hg^{II} [77]. When a small amount (0.16 ppt) of Hg^0 is added to the 0D box model, along with the Hg-halogen mechanism from Shah *et al*Shah, Jacob, Thackray, Wang, Sunderland, Dibble, Saiz-Lopez, Černušák, Kellö, Castro, Wu and Wang [13], we find roughly 90% conversion to oxidized forms of Hg within 10 minutes (Figure S17). This halogen-induced oxidation may explain the observed increases in Hg^{II}. However, because these observations did not coincide temporally or spatially with the UWFPS campaign, we don't attempt to further constrain our model to these observations.

The second additional note is that while many of the reactions of Br and Cl radicals are hydrogen abstraction reactions with saturated carbon bonds, the reactions of halogen radicals with small alkenes proceed via addition across the double bond, inserting the halogen into the VOC. The box model explicitly models this detailed chemistry, and predicts that at the end of the six hours, the average plume will contain 250 ppt chlorinated VOCs (mostly chloroaldehyde, formyl chloride and chloro-PAN) and 120 ppt brominated VOCS (mostly bromoaldehyde, bromopropylperoxide, and 2-bromopropanal). Halogenated VOCs are known air and water toxins[78], but most research has focused on the health impacts of chlorinated alkanes, alkenes, and aromatics. The impact of these halogenated oxidized VOCs is unclear and merits further study.

443 The third aspect is that no iodine species could be quantified during UWFPS, but if
444 molecular iodine (I_2) or iodide halogens (ICl or IBr) are also emitted by US Magnesium as an
445 impurity in the same manner as BrCl and Br_2, I and IO radicals would serve as an even more potent
446 oxidizing species than bromine. However, rates and mechanisms for the reactions of iodine with
447 VOCs are even less certain that those of bromine. Future targeted studies including explicit
448 measurement of IO or other iodine compounds could address these uncertainties.
449
450 IV. Implications for air quality
451 We observed large quantities of halogens in the plumes emanating from the US Magnesium
452 plant on the southwest edge of the Great Salt Lake using an instrumented aircraft. The transported
453 and diluted plumes were observed throughout the populated Great Salt Lake Basin. We used the
454 aircraft measurements to estimate the emissions of Cl_2, HCl, and NO_x, and found them to be in
455 agreement with those stack emissions reported in the Toxic Release Inventory for the US
456 Magnesium facility. We also found substantial Br_2 and BrCl emissions, which are an unreported
457 and potentially major source of anthropogenic pollutants. We constructed a photochemical box
458 model, constrained to daytime observations, to reproduce the frequent O_3 depletion seen in all
459 daytime plumes in the near-field, and confirmed that halogen-induced O_3 depletion is the dominant
460 chemical mechanism. Finally, we used both the box model and a 3D atmospheric chemistry model
461 to estimate the effect of the US Magnesium halogen emissions on downwind particulate nitrate
462 build-up in populated regions and find that emissions from this single industrial halogen point
463 source are associated with increases in $PM_{2.5}$ throughout the populated areas surrounding the Great
464 Salt Lake.

Halogens affect the oxidative capacity of the atmosphere[45, 79-81] and the build-up of haze pollution in populated areas[9, 10, 82] but tracking the chemical transformations following high levels of halogen emissions from a point source has few precedents, such as in Lee *et al*[32]. While the role of particulate chloride in $PM_{2.5}$ formation has long been a cause for concern in the Salt Lake Basin[26, 73], these results demonstrate an additional role of chlorine and bromine radicals beyond adding particulate mass through the uptake of HCl and $ClNO_2$ onto aerosol. The introduction of the Br and Cl radicals increases the production of oxidized VOCs and nitric acid, thereby increasing the cycling through the HO_x-NO_x cycle, which is oxidant-limited in the winter. This is consistent with previous results in urban areas in East Asia[9]. The observations from UWFPS therefore provide a unique opportunity to examine the role that industrial halogens have on a polluted urban area, and can help constrain our current understanding of tropospheric halogen chemistry. Magnesium refineries are not common, but exist in several countries including the US, China, Russia, and Israel[83], and quantifying the halogen emissions from these plants could clarify the effect of their emissions on air quality compared to other local and natural sources of halogens. Lithium extraction from geothermal salt brines has been proposed to meet the increasing demand for battery power, and could represent an additional source of halogenated species[84]. Halogen oxides (BrO, ClO, and IO) have absorption features in the UV-visible wavelength range[85], and therefore observations from satellites can identify possible hotspots of halogen emissions from industrial sources.

Finally, we note that the Great Salt Lake area is also in nonattainment for summertime ozone. Previous modeling has demonstrated that the photochemical cycles leading to O_3 and ammonium nitrate are linked[30]. Further observation and modeling investigations may identify additional air quality impacts associated with this large halogen source in other seasons.

ASSOCIATED CONTENT

Supporting Information.

The Supporting Information (PDF) contains supplemental text, figures, and tables that describe additional model details, instrumentation details, the full chemical mechanism, sensitivity tests, and further model outputs.

AUTHOR INFORMATION

Corresponding Author

*Caroline Womack: caroline.womack@noaa.gov

Present Addresses

[†]W.S.C.: Now at Department of Chemistry, University of Colorado, and NOAA Chemical Sciences Laboratory, Boulder, CO, 80305, United States

[‡]D.L.F.: Now at California Air Resources Board, Sacramento, CA, 95814, United States

[#]A.F.: Now at National Center for Atmospheric Research, Boulder, CO, 80307, United States

[§]L.G.: Now at Pacific Northwest National Laboratory, Richland, WA, 99354, United States

[¶]E.E.M.: Now at Department of Energy, Environmental, and Chemical Engineering, Washington University in St. Louis, MO, 63130, United States

[‖]A.M.: Now at German Environment Agency, Department of Air Quality, 06844 Dessau-Roßlau, Germany

Author Contributions

MB, SSB, and JCL conceived of the UWFPS campaign. CCW, DLF, LG, JAT, EEM, AF, AMM, AM, JGM, and SSB collected the data on the NOAA Twin Otter. BL processed the CIMS data. JAN and PRV aided the CIMS calibration. CCW, WC, and DLF analyzed the aircraft data and constructed the box model. SY, BCM, CH, and DSJ performed the 3-D modeling. CCW wrote the manuscript. All authors contributed to editing the manuscript.

Funding Sources

The CAM-chem/MUSICA simulations were performed on the Cheyenne supercomputer (doi:10.5065/D6RX99HX) provided by the National Center for Atmospheric Research, which is a major facility sponsored by the NSF under Cooperative Agreement 1852977. CCW, DF, EM, and AF were partially supported by the NOAA Cooperative Agreement with CIRES, NA17OAR4320101. WC was supported by the NOAA Hollings Program.

ACKNOWLEDGMENT: We acknowledge support from the Utah Department of Air Quality under award #210517, and thank Christopher Pennell for award administration and discussion of results. We would like to thank Jim Roberts and Wayne Angevine for helpful discussions, and the NOAA Aircraft Operations Center. The data analysis code and F0AM halogen mechanism can be found at https://csl.noaa.gov/groups/csl7/measurements/2017uwfps/pubs/. The UWFPS data is at: https://csl.noaa.gov/groups/csl7/measurements/2017uwfps/TwinOtter/DataDownload/. The STILT data is at: https://home.chpc.utah.edu/~lin/UWFPS_STILT/STILT_foot_trajs/.

REFERENCES

Uncategorized References

(1) Simpson, W. R.; Brown, S. S.; Saiz-Lopez, A.; Thornton, J. A.; von Glasow, R. Tropospheric Halogen Chemistry: Sources, Cycling, and Impacts. *Chem. Rev.* **2015**, *115* (10), 4035-4062. DOI: https://doi.org/10.1021/cr5006638.

(2) Saiz-Lopez, A.; von Glasow, R. Reactive halogen chemistry in the troposphere. *Chem. Soc. Rev.* **2012**, *41* (19), 6448-6472. DOI: https://doi.org/10.1039/C2CS35208G.
(3) Lary, D. J. Catalytic destruction of stratospheric ozone. *J. Geophys. Res.* **1997**, *102* (D17), 21515-21526. DOI: https://doi.org/10.1029/97JD00912.
(4) Thompson, C. R.; Shepson, P. B.; Liao, J.; Huey, L. G.; Cantrell, C.; Flocke, F.; Orlando, J. Bromine atom production and chain propagation during springtime Arctic ozone depletion events in Barrow, Alaska. *Atmos. Chem. Phys.* **2017**, *17* (5), 3401-3421. DOI: https://doi.org/10.5194/acp-17-3401-2017.
(5) Finlayson-Pitts, B. J.; Ezell, M. J.; Pitts, J. N. Formation of chemically active chlorine compounds by reactions of atmospheric NaCl particles with gaseous N2O5 and ClONO2. *Nature* **1989**, *337* (6204), 241-244. DOI: https://doi.org/10.1038/337241a0.
(6) Osthoff, H. D.; Roberts, J. M.; Ravishankara, A. R.; Williams, E. J.; Lerner, B. M.; Sommariva, R.; Bates, T. S.; Coffman, D.; Quinn, P. K.; Dibb, J. E.; et al. High levels of nitryl chloride in the polluted subtropical marine boundary layer. *Nat. Geosci.* **2008**, *1* (5), 324-328. DOI: http://doi.org/10.1038/ngeo177.
(7) Thornton, J. A.; Kercher, J. P.; Riedel, T. P.; Wagner, N. L.; Cozic, J.; Holloway, J. S.; Dubé, W. P.; Wolfe, G. M.; Quinn, P. K.; Middlebrook, A. M.; et al. A large atomic chlorine source inferred from mid-continental reactive nitrogen chemistry. *Nature* **2010**, *464* (7286), 271-274. DOI: https://doi.org/10.1038/nature08905.
(8) Riedel, T. P.; Wolfe, G. M.; Danas, K. T.; Gilman, J. B.; Kuster, W. C.; Bon, D. M.; Vlasenko, A.; Li, S. M.; Williams, E. J.; Lerner, B. M.; et al. An MCM modeling study of nitryl chloride ($ClNO_2$) impacts on oxidation, ozone production and nitrogen oxide partitioning in polluted continental outflow. *Atmos. Chem. Phys.* **2014**, *14* (8), 3789-3800. DOI: https://doi.org/10.5194/acp-14-3789-2014.
(9) Peng, X.; Wang, W.; Xia, M.; Chen, H.; Ravishankara, A. R.; Li, Q.; Saiz-Lopez, A.; Liu, P.; Zhang, F.; Zhang, C.; et al. An unexpected large continental source of reactive bromine and chlorine with significant impact on wintertime air quality. *Natl. Sci. Rev.* **2020**, *8* (7), nwaa304. DOI: https://doi.org/10.1093/nsr/nwaa304.
(10) Li, Q.; Fu, X.; Peng, X.; Wang, W.; Badia, A.; Fernandez, R. P.; Cuevas, C. A.; Mu, Y.; Chen, J.; Jimenez, J. L.; et al. Halogens Enhance Haze Pollution in China. *Environ. Sci. Technol.* **2021**, *55* (20), 13625-13637. DOI: https://doi.org/10.1021/acs.est.1c01949.
(11) Fan, X.; Cai, J.; Yan, C.; Zhao, J.; Guo, Y.; Li, C.; Dällenbach, K. R.; Zheng, F.; Lin, Z.; Chu, B.; et al. Atmospheric gaseous hydrochloric and hydrobromic acid in urban Beijing, China: detection, source identification and potential atmospheric impacts. *Atmos. Chem. Phys.* **2021**, *21* (14), 11437-11452. DOI: https://doi.org/10.5194/acp-21-11437-2021.
(12) Dibble, T. S.; Tetu, H. L.; Jiao, Y.; Thackray, C. P.; Jacob, D. J. Modeling the OH-Initiated Oxidation of Mercury in the Global Atmosphere without Violating Physical Laws. *J. Phys. Chem. A* **2020**, *124* (2), 444-453. DOI: https://doi.org/10.1021/acs.jpca.9b10121.
(13) Shah, V.; Jacob, D. J.; Thackray, C. P.; Wang, X.; Sunderland, E. M.; Dibble, T. S.; Saiz-Lopez, A.; Černušák, I.; Kellö, V.; Castro, P. J.; et al. Improved Mechanistic Model of the Atmospheric Redox Chemistry of Mercury. *Environ. Sci. Technol.* **2021**, *55* (21), 14445-14456. DOI: https://doi.org/10.1021/acs.est.1c03160.
(14) Muñiz-Unamunzaga, M.; Borge, R.; Sarwar, G.; Gantt, B.; de la Paz, D.; Cuevas, C. A.; Saiz-Lopez, A. The influence of ocean halogen and sulfur emissions in the air quality of a coastal megacity: The case of Los Angeles. *Sci. Total Environ.* **2018**, *610-611*, 1536-1545. DOI: https://doi.org/10.1016/j.scitotenv.2017.06.098.

(15) Hebestreit, K.; Stutz, J.; Rosen, D.; Matveiv, V.; Peleg, M.; Luria, M.; Platt, U. DOAS Measurements of Tropospheric Bromine Oxide in Mid-Latitudes. *Science* **1999**, *283* (5398), 55-57. DOI: https://doi.org/10.1126/science.283.5398.55.
(16) Matveev, V.; Peleg, M.; Rosen, D.; Tov-Alper, D. S.; Hebestreit, K.; Stutz, J.; Platt, U.; Blake, D.; Luria, M. Bromine oxide—ozone interaction over the Dead Sea. *J. Geophys. Res.* **2001**, *106* (D10), 10375-10387. DOI: https://doi.org/10.1029/2000JD900611.
(17) Tas, E.; Peleg, M.; Matveev, V.; Zingler, J.; Luria, M. Frequency and extent of bromine oxide formation over the Dead Sea. *J. Geophys. Res.* **2005**, *110* (D11), D11304. DOI: https://doi.org/10.1029/2004JD005665.
(18) Holla, R.; Schmitt, S.; Zingler, U. F.; Pöhler, D.; Zingler, J.; Corsmeier, U.; Platt, U. Vertical distribution of BrO in the boundary layer at the Dead Sea. *Environ. Chem.* **2015**, *12* (4), 438-460. DOI: http://doi.org/10.1071/EN14224.
(19) Hörmann, C.; Sihler, H.; Beirle, S.; Penning de Vries, M.; Platt, U.; Wagner, T. Seasonal variation of tropospheric bromine monoxide over the Rann of Kutch salt marsh seen from space. *Atmos. Chem. Phys.* **2016**, *16* (20), 13015-13034. DOI: https://doi.org/10.5194/acp-16-13015-2016.
(20) Hönninger, G.; Bobrowski, N.; Palenque, E. R.; Torrez, R.; Platt, U. Reactive bromine and sulfur emissions at Salar de Uyuni, Bolivia. *Geophys. Res. Lett.* **2004**, *31* (4), L04101. DOI: https://doi.org/10.1029/2003GL018818.
(21) Stutz, J.; Ackermann, R.; Fast, J. D.; Barrie, L. Atmospheric reactive chlorine and bromine at the Great Salt Lake, Utah. *Geophys. Res. Lett.* **2002**, *29* (10), 18. DOI: https://doi.org/10.1029/2002gl014812.
(22) Pletcher, K. Dead Sea. In *Encyclopedia Britannica*, 2016; Updated 2022-10-25.
(23) White, J. S.; Null, S. E.; Tarboton, D. *More than Meets the Eye: Managing Salinity in Great Salt Lake, Utah*; Lakelines Magazine, 2014. https://hydrology.usu.edu/dtarb/White_etal_2014_Lakeline.pdf (accessed 2022-11-28).
(24) Toxic Release Inventory database. US Environmental Protection Agency. https://www.epa.gov/toxics-release-inventory-tri-program/tri-data-and-tools#tridata-facilities (accessed 2022-11-28).
(25) Baasandorj, M.; Brown, S. S.; Hoch, S.; Crosman, E.; Long, R.; Silva, P.; L., M.; I., H.; Martin, R.; R., B.; et al. *2017 Utah Winter Fine Particulate Study Final Report*; 2018. https://www.esrl.noaa.gov/csd/groups/csd7/measurements/2017uwfps/finalreport.pdf (accessed 2022-11-28).
(26) Baasandorj, M.; Hoch, S. W.; Bares, R.; Lin, J. C.; Brown, S. S.; Millet, D. B.; Martin, R.; Kelly, K.; Zarzana, K. J.; Whiteman, C. D.; et al. Coupling between Chemical and Meteorological Processes under Persistent Cold-Air Pool Conditions: Evolution of Wintertime $PM_{2.5}$ Pollution Events and N_2O_5 Observations in Utah's Salt Lake Valley. *Environ. Sci. Technol.* **2017**, *51* (11), 5941-5950. DOI: http://doi.org/10.1021/acs.est.6b06603.
(27) Franchin, A.; Fibiger, D. L.; Goldberger, L.; McDuffie, E. E.; Moravek, A.; Womack, C. C.; Crosman, E. T.; Docherty, K. S.; Dube, W. P.; Hoch, S. W.; et al. Airborne and ground-based observations of ammonium nitrate dominated aerosols in a shallow boundary layer during intense winter pollution episodes in northern Utah. *Atmos. Chem. Phys.* **2018**, *18*, 17259-17276. DOI: http://doi.org/10.5194/acp-18-17259-2018.
(28) McDuffie, E. E.; Womack, C. C.; Fibiger, D. L.; Dube, W. P.; Franchin, A.; Middlebrook, A. M.; Goldberger, L.; Lee, B. H.; Thornton, J. A.; Moravek, A.; et al. On the contribution of nocturnal heterogeneous reactive nitrogen chemistry to particulate matter formation during

wintertime pollution events in Northern Utah. *Atmos. Chem. Phys.* **2019**, *19* (14), 9287-9308. DOI: https://doi.org/10.5194/acp-19-9287-2019.
(29) Moravek, A.; Murphy, J. G.; Hrdina, A.; Lin, J. C.; Pennell, C.; Franchin, A.; Middlebrook, A. M.; Fibiger, D. L.; Womack, C. C.; McDuffie, E. E.; et al. Wintertime spatial distribution of ammonia and its emission sources in the Great Salt Lake region. *Atmos. Chem. Phys.* **2019**, *19* (24), 15691-15709. DOI: https://doi.org/10.5194/acp-19-15691-2019.
(30) Womack, C. C.; McDuffie, E. E.; Edwards, P. M.; Bares, R.; de Gouw, J. A.; Docherty, K. S.; Dubé, W. P.; Fibiger, D. L.; Franchin, A.; Gilman, J. B.; et al. An Odd Oxygen Framework for Wintertime Ammonium Nitrate Aerosol Pollution in Urban Areas: NO_x and VOC Control as Mitigation Strategies. *Geophys. Res. Lett.* **2019**, *46* (9), 4971-4979. DOI: https://doi.org/10.1029/2019gl082028.
(31) Lee, B. H.; Lopez-Hilfiker, F. D.; Mohr, C.; Kurtén, T.; Worsnop, D. R.; Thornton, J. A. An iodide-adduct high-resolution time-of-flight chemical-ionization mass spectrometer: Application to atmospheric inorganic and organic compounds. *Environ. Sci. Technol.* **2014**, *48* (11), 6309-6317. DOI: http://doi.org/10.1021/es500362a.
(32) Lee, B. H.; Lopez-Hilfiker, F. D.; Veres, P. R.; McDuffie, E. E.; Fibiger, D. L.; Sparks, T. L.; Ebben, C. J.; Green, J. R.; Schroder, J. C.; Campuzano-Jost, P.; et al. Flight Deployment of a High-Resolution Time-of-Flight Chemical Ionization Mass Spectrometer: Observations of Reactive Halogen and Nitrogen Oxide Species. *J. Geophys. Res. - Atmos.* **2018**, *123* (14), 7670-7686. DOI: https://doi.org/10.1029/2017JD028082.
(33) Iyer, S.; Lopez-Hilfiker, F.; Lee, B. H.; Thornton, J. A.; Kurtén, T. Modeling the Detection of Organic and Inorganic Compounds Using Iodide-Based Chemical Ionization. *J. Phys. Chem. A* **2016**, *120* (4), 576-587. DOI: https://doi.org/10.1021/acs.jpca.5b09837.
(34) Wild, R. J.; Edwards, P. M.; Dubé, W. P.; Baumann, K.; Edgerton, E. S.; Quinn, P. K.; Roberts, J. M.; Rollins, A. W.; Veres, P. R.; Warneke, C.; et al. A measurement of total reactive nitrogen, NO_y, together with NO_2, NO, and O_3 via cavity ring-down spectroscopy. *Environ. Sci. Technol.* **2014**, *48* (16), 9609-9615. DOI: http://doi.org/10.1021/es501896w.
(35) Bahreini, R.; Dunlea, E. J.; Matthew, B. M.; Simons, C.; Docherty, K. S.; DeCarlo, P. F.; Jimenez, J. L.; Brock, C. A.; Middlebrook, A. M. Design and operation of a pressure-controlled inlet for airborne sampling with an aerodynamic aerosol lens. *Aerosol Sci. Tech.* **2008**, *42* (6), 465-471. DOI: https://doi.org/10.1080/02786820802178514.
(36) Liao, J.; Brock, C. A.; Murphy, D. M.; Sueper, D. T.; Welti, A.; Middlebrook, A. M. Single-particle measurements of bouncing particles and in situ collection efficiency from an airborne aerosol mass spectrometer (AMS) with light-scattering detection. *Atmos. Meas. Tech.* **2017**, *10* (10), 3801-3820. DOI: http://doi.org/10.5194/amt-10-3801-2017.
(37) Kupc, A.; Williamson, C.; Wagner, N. L.; Richardson, M.; Brock, C. A. Modification, calibration, and performance of the Ultra-High Sensitivity Aerosol Spectrometer for particle size distribution and volatility measurements during the Atmospheric Tomography Mission (ATom) airborne campaign. *Atmos. Meas. Tech.* **2018**, *11* (1), 369-383. DOI: https://doi.org/10.5194/amt-11-369-2018.
(38) Lin, J. C.; Gerbig, C.; Wofsy, S. C.; Andrews, A. E.; Daube, B. C.; Davis, K. J.; Grainger, C. A. A near-field tool for simulating the upstream influence of atmospheric observations: The Stochastic Time-Inverted Lagrangian Transport (STILT) model. *J. Geophys. Res.* **2003**, *108* (D16), 4493. DOI: https://doi.org/10.1029/2002JD003161.
(39) High-Resolution Rapid Refresh available at:. https://rapidrefresh.noaa.gov/hrrr/ (accessed 2022-11-28).

(40) Peischl, J.; Ryerson, T. B.; Aikin, K. C.; de Gouw, J. A.; Gilman, J. B.; Holloway, J. S.; Lerner, B. M.; Nadkarni, R.; Neuman, J. A.; Nowak, J. B.; et al. Quantifying atmospheric methane emissions from the Haynesville, Fayetteville, and northeastern Marcellus shale gas production regions. *J. Geophys. Res. - Atmos.* **2015**, *120* (5), 2119-2139. DOI: https://doi.org/10.1002/2014jd022697.
(41) White, W.; Anderson, J.; Blumenthal, D.; Husar, R.; Gillani, N.; Husar, J.; Wilson, W. Formation and transport of secondary air pollutants: ozone and aerosols in the St. Louis urban plume. *Science* **1976**, *194* (4261), 187-189. DOI: https://doi.org/10.1126/science.959846.
(42) Peischl, J.; Ryerson, T. B.; Holloway, J. S.; Parrish, D. D.; Trainer, M.; Frost, G. J.; Aikin, K. C.; Brown, S. S.; Dubé, W. P.; Stark, H.; et al. A top-down analysis of emissions from selected Texas power plants during TexAQS 2000 and 2006. *J. Geophys. Res.* **2010**, *115* (D16), D16303. DOI: https://doi.org/10.1029/2009JD013527.
(43) Wolfe, G. M.; Marvin, M. R.; Roberts, S. J.; Travis, K. R.; Liao, J. The Framework for 0-D Atmospheric Modeling (F0AM) v3.1. *Geosci. Model Dev.* **2016**, *9* (9), 3309-3319. DOI: https://doi.org/10.5194/gmd-9-3309-2016.
(44) Jenkin, M. E.; Young, J. C.; Rickard, A. R. The MCM v3.3.1 degradation scheme for isoprene. *Atmos. Chem. Phys.* **2015**, *15* (20), 11433-11459. DOI: http://doi.org/10.5194/acp-15-11433-2015.
(45) Sherwen, T.; Schmidt, J. A.; Evans, M. J.; Carpenter, L. J.; Großmann, K.; Eastham, S. D.; Jacob, D. J.; Dix, B.; Koenig, T. K.; Sinreich, R.; et al. Global impacts of tropospheric halogens (Cl, Br, I) on oxidants and composition in GEOS-Chem. *Atmos. Chem. Phys.* **2016**, *16* (18), 12239-12271. DOI: https://doi.org/10.5194/acp-16-12239-2016.
(46) Badia, A.; Reeves, C. E.; Baker, A. R.; Saiz-Lopez, A.; Volkamer, R.; Koenig, T. K.; Apel, E. C.; Hornbrook, R. S.; Carpenter, L. J.; Andrews, S. J.; et al. Importance of reactive halogens in the tropical marine atmosphere: a regional modelling study using WRF-Chem. *Atmos. Chem. Phys.* **2019**, *19* (5), 3161-3189. DOI: https://doi.org/10.5194/acp-19-3161-2019.
(47) Romer, P. S.; Wooldridge, P. J.; Crounse, J. D.; Kim, M. J.; Wennberg, P. O.; Dibb, J. E.; Scheuer, E.; Blake, D. R.; Meinardi, S.; Brosius, A. L.; et al. Constraints on Aerosol Nitrate Photolysis as a Potential Source of HONO and NO_x. *Environ. Sci. Technol.* **2018**, *52* (23), 13738-13746. DOI: https://doi.org/10.1021/acs.est.8b03861.
(48) Chemical kinetics and photochemical data for use in atmospheric studies. Evaluation No. 17 http://jpldataeval.jpl.nasa.gov/ (accessed 2022-11-28).
(49) Atkinson, R.; Baulch, D. L.; Cox, R. A.; Crowley, J. N.; Hampson, R. F.; Hynes, R. G.; Jenkin, M. E.; Rossi, M. J.; Troe, J. Evaluated kinetic and photochemical data for atmospheric chemistry: Volume III - gas phase reactions of inorganic halogens. *Atmos. Chem. Phys.* **2007**, *7* (4), 981-1191. DOI: https://doi.org/10.5194/acp-7-981-2007.
(50) Atkinson, R.; Baulch, D. L.; Cox, R. A.; Crowley, J. N.; Hampson, R. F.; Hynes, R. G.; Jenkin, M. E.; Rossi, M. J.; Troe, J.; Subcommittee, I. Evaluated kinetic and photochemical data for atmospheric chemistry: Volume II - gas phase reactions of organic species. *Atmos. Chem. Phys.* **2006**, *6* (11), 3625-4055. DOI: https://doi.org/10.5194/acp-6-3625-2006.
(51) Atkinson, R.; Baulch, D. L.; Cox, R. A.; Crowley, J. N.; Hampson, R. F.; Hynes, R. G.; Jenkin, M. E.; Rossi, M. J.; Troe, J.; Wallington, T. J. Evaluated kinetic and photochemical data for atmospheric chemistry: Volume IV – gas phase reactions of organic halogen species. *Atmos. Chem. Phys.* **2008**, *8* (15), 4141-4496. DOI: https://doi.org/10.5194/acp-8-4141-2008.

(52) Xue, L. K.; Saunders, S. M.; Wang, T.; Gao, R.; Wang, X. F.; Zhang, Q. Z.; Wang, W. X. Development of a chlorine chemistry module for the Master Chemical Mechanism. *Geosci. Model Dev.* **2015**, *8* (10), 3151-3162. DOI: https://doi.org/10.5194/gmd-8-3151-2015.
(53) Shi, J.; Bernhard, M. J. Kinetic studies of Cl-atom reactions with selected aromatic compounds using the photochemical reactor-FTIR spectroscopy technique. *Int. J. Chem. Kinet.* **1997**, *29* (5), 349-358. DOI: https://doi.org/10.1002/(SICI)1097-4601(1997)29:5<349::AID-KIN5>3.0.CO;2-U.
(54) Orlando, J. J.; Tyndall, G. S. Rate Coefficients for the Thermal Decomposition of $BrONO_2$ and the Heat of Formation of $BrONO_2$. *J. Phys. Chem.* **1996**, *100* (50), 19398-19405. DOI: https://doi.org/10.1021/jp9620274.
(55) King, K. D.; Golden, D. M.; Benson, S. W. Kinetics of the gas-phase thermal bromination of acetone. Heat of formation and stabilization energy of the acetonyl radical. *J. Am. Chem. Soc.* **1970**, *92* (19), 5541-5546. DOI: https://doi.org/10.1021/ja00722a001.
(56) Seakins, P. W.; Pilling, M. J.; Niiranen, J. T.; Gutman, D.; Krasnoperov, L. N. Kinetics and thermochemistry of R + hydrogen bromide ↔ RH + bromine atom reactions: determinations of the heat of formation of ethyl, isopropyl, sec-butyl and tert-butyl radicals. *J. Phys. Chem.* **1992**, *96* (24), 9847-9855. DOI: https://doi.org/10.1021/j100203a050.
(57) Wolfe, G. M.; Hanisco, T. F.; Arkinson, H. L.; Blake, D. R.; Wisthaler, A.; Mikoviny, T.; Ryerson, T. B.; Pollack, I.; Peischl, J.; Wennberg, P. O.; et al. Photochemical evolution of the 2013 California Rim Fire: synergistic impacts of reactive hydrocarbons and enhanced oxidants. *Atmos. Chem. Phys.* **2022**, *22* (6), 4253-4275. DOI: https://doi.org/10.5194/acp-22-4253-2022.
(58) Gilman, J. B.; Lerner, B. M.; Kuster, W. C.; de Gouw, J. A. Source Signature of Volatile Organic Compounds from Oil and Natural Gas Operations in Northeastern Colorado. *Environ. Sci. Technol.* **2013**, *47* (3), 1297-1305. DOI: https://doi.org/10.1021/es304119a.
(59) Lamarque, J. F.; Emmons, L. K.; Hess, P. G.; Kinnison, D. E.; Tilmes, S.; Vitt, F.; Heald, C. L.; Holland, E. A.; Lauritzen, P. H.; Neu, J.; et al. CAM-chem: description and evaluation of interactive atmospheric chemistry in the Community Earth System Model. *Geosci. Model Dev.* **2012**, *5* (2), 369-411. DOI: https://doi.org/10.5194/gmd-5-369-2012.
(60) Emmons, L. K.; Schwantes, R. H.; Orlando, J. J.; Tyndall, G.; Kinnison, D.; Lamarque, J.-F.; Marsh, D.; Mills, M. J.; Tilmes, S.; Bardeen, C.; et al. The Chemistry Mechanism in the Community Earth System Model Version 2 (CESM2). *J. Adv. Model Earth Sy.* **2020**, *12* (4), e2019MS001882. DOI: https://doi.org/10.1029/2019MS001882.
(61) Pfister, G. G.; Eastham, S. D.; Arellano, A. F.; Aumont, B.; Barsanti, K. C.; Barth, M. C.; Conley, A.; Davis, N. A.; Emmons, L. K.; Fast, J. D.; et al. The Multi-Scale Infrastructure for Chemistry and Aerosols (MUSICA). *B. Am. Meterol. Soc.* **2020**, *101* (10), E1743-E1760. DOI: https://doi.org/10.1175/bams-d-19-0331.1.
(62) Schwantes, R. H.; Lacey, F. G.; Tilmes, S.; Emmons, L. K.; Lauritzen, P. H.; Walters, S.; Callaghan, P.; Zarzycki, C. M.; Barth, M. C.; Jo, D. S.; et al. Evaluating the Impact of Chemical Complexity and Horizontal Resolution on Tropospheric Ozone Over the Conterminous US With a Global Variable Resolution Chemistry Model. *J. Adv. Model Earth Sy.* **2022**, *14* (6), e2021MS002889. DOI: https://doi.org/10.1029/2021MS002889.
(63) Gelaro, R.; McCarty, W.; Suárez, M. J.; Todling, R.; Molod, A.; Takacs, L.; Randles, C. A.; Darmenov, A.; Bosilovich, M. G.; Reichle, R.; et al. The Modern-Era Retrospective Analysis for Research and Applications, Version 2 (MERRA-2) *J. Climate* **2017**, *30* (14), 5419-5454. DOI: https://doi.org/10.1175/jcli-d-16-0758.1.

(64) Wang, S.; Kinnison, D.; Montzka, S. A.; Apel, E. C.; Hornbrook, R. S.; Hills, A. J.; Blake, D. R.; Barletta, B.; Meinardi, S.; Sweeney, C.; et al. Ocean Biogeochemistry Control on the Marine Emissions of Brominated Very Short-Lived Ozone-Depleting Substances: A Machine-Learning Approach. *J. Geophys. Res. - Atmos.* **2019**, *124* (22), 12319-12339. DOI: https://doi.org/10.1029/2019JD031288.
(65) Liu, X.; Ma, P. L.; Wang, H.; Tilmes, S.; Singh, B.; Easter, R. C.; Ghan, S. J.; Rasch, P. J. Description and evaluation of a new four-mode version of the Modal Aerosol Module (MAM4) within version 5.3 of the Community Atmosphere Model. *Geosci. Model Dev.* **2016**, *9* (2), 505-522. DOI: https://doi.org/10.5194/gmd-9-505-2016.
(66) Fung, K. M.; Heald, C. L.; Kroll, J. H.; Wang, S.; Jo, D. S.; Gettelman, A.; Lu, Z.; Liu, X.; Zaveri, R. A.; Apel, E. C.; et al. Exploring dimethyl sulfide (DMS) oxidation and implications for global aerosol radiative forcing. *Atmos. Chem. Phys.* **2022**, *22* (2), 1549-1573. DOI: https://doi.org/10.5194/acp-22-1549-2022.
(67) Zaveri, R. A.; Easter, R. C.; Singh, B.; Wang, H.; Lu, Z.; Tilmes, S.; Emmons, L. K.; Vitt, F.; Zhang, R.; Liu, X.; et al. Development and Evaluation of Chemistry-Aerosol-Climate Model CAM5-Chem-MAM7-MOSAIC: Global Atmospheric Distribution and Radiative Effects of Nitrate Aerosol. *J. Adv. Model Earth Sy.* **2021**, *13* (4), e2020MS002346. DOI: https://doi.org/10.1029/2020MS002346.
(68) Granier, C.; Darras, S.; Gon, H. D. v. d.; Doubalova, J.; Elguindi, N.; Galle, B.; Gauss, M.; M.Guevara; Jalkanen, J.-P.; Kuenen, J.; et al. *The Copernicus Atmosphere Monitoring Service global and regional emissions (April 2019 version), Copernicus Atmosphere Monitoring Service (CAMS) report.* ; 2019. (accessed 2022-11-28). DOI: https://doi.org/10.24380/d0bn-kx16.
(69) Li, M.; McDonald, B. C.; McKeen, S. A.; Eskes, H.; Levelt, P.; Francoeur, C.; Harkins, C.; He, J.; Barth, M.; Henze, D. K.; et al. Assessment of Updated Fuel-Based Emissions Inventories Over the Contiguous United States Using TROPOMI NO_2 Retrievals. *J. Geophys. Res. - Atmos.* **2021**, *126* (24), e2021JD035484. DOI: https://doi.org/10.1029/2021JD035484.
(70) Francoeur, C. B.; McDonald, B. C.; Gilman, J. B.; Zarzana, K. J.; Dix, B.; Brown, S. S.; de Gouw, J. A.; Frost, G. J.; Li, M.; McKeen, S. A.; et al. Quantifying Methane and Ozone Precursor Emissions from Oil and Gas Production Regions across the Contiguous US. *Environ. Sci. Technol.* **2021**, *55* (13), 9129-9139. DOI: https://doi.org/10.1021/acs.est.0c07352.
(71) National Emissions Inventory. US Environmental Protection Agency. https://www.epa.gov/air-emissions-inventories/2017-national-emissions-inventory-nei-data#datas (accessed 2022-11-28).
(72) Zelenski, M.; Taran, Y. Volcanic emissions of molecular chlorine. *Geochim. Cosmochim. Ac.* **2012**, *87*, 210-226. DOI: https://doi.org/10.1016/j.gca.2012.03.034.
(73) Kelly, K. E.; Kotchenruther, R.; Kuprov, R.; Silcox, G. D. Receptor model source attributions for Utah's Salt Lake City airshed and the impacts of wintertime secondary ammonium nitrate and ammonium chloride aerosol. *J. Air. Waste. Manage. Assoc.* **2013**, *63* (5), 575-590. DOI: http://doi.org/10.1080/10962247.2013.774819.
(74) Silcox, G. D.; Kelly, K. E.; Crosman, E. T.; Whiteman, C. D.; Allen, B. L. Wintertime $PM_{2.5}$ concentrations during persistent, multi-day cold-air pools in a mountain valley. *Atmos. Environ.* **2012**, *46*, 17-24. DOI: http://doi.org/10.1016/j.atmosenv.2011.10.041.
(75) Horowitz, H. M.; Jacob, D. J.; Zhang, Y.; Dibble, T. S.; Slemr, F.; Amos, H. M.; Schmidt, J. A.; Corbitt, E. S.; Marais, E. A.; Sunderland, E. M. A new mechanism for atmospheric mercury redox chemistry: implications for the global mercury budget. *Atmos. Chem. Phys.* **2017**, *17* (10), 6353-6371. DOI: https://doi.org/10.5194/acp-17-6353-2017.

(76) The National Atmospheric Deposition Program's Atmospheric Mecury Network (AMNet). https://nadp.slh.wisc.edu/networks/atmospheric-mercury-network/ (accessed 2022-11-28).
(77) Lan, X.; Talbot, R.; Castro, M.; Perry, K.; Luke, W. Seasonal and diurnal variations of atmospheric mercury across the US determined from AMNet monitoring data. *Atmos. Chem. Phys.* **2012**, *12* (21), 10569-10582. DOI: https://doi.org/10.5194/acp-12-10569-2012.
(78) Huang, B.; Lei, C.; Wei, C.; Zeng, G. Chlorinated volatile organic compounds (Cl-VOCs) in environment — sources, potential human health impacts, and current remediation technologies. *Environ. Int.* **2014**, *71*, 118-138. DOI: https://doi.org/10.1016/j.envint.2014.06.013.
(79) Stone, D.; Sherwen, T.; Evans, M. J.; Vaughan, S.; Ingham, T.; Whalley, L. K.; Edwards, P. M.; Read, K. A.; Lee, J. D.; Moller, S. J.; et al. Impacts of bromine and iodine chemistry on tropospheric OH and HO_2: comparing observations with box and global model perspectives. *Atmos. Chem. Phys.* **2018**, *18* (5), 3541-3561. DOI: https://doi.org/10.5194/acp-18-3541-2018.
(80) Sherwen, T.; Evans, M. J.; Carpenter, L. J.; Schmidt, J. A.; Mickley, L. J. Halogen chemistry reduces tropospheric O_3 radiative forcing. *Atmos. Chem. Phys.* **2017**, *17* (2), 1557-1569. DOI: https://doi.org/10.5194/acp-17-1557-2017.
(81) Wang, X.; Jacob, D. J.; Downs, W.; Zhai, S.; Zhu, L.; Shah, V.; Holmes, C. D.; Sherwen, T.; Alexander, B.; Evans, M. J.; et al. Global tropospheric halogen (Cl, Br, I) chemistry and its impact on oxidants. *Atmos. Chem. Phys.* **2021**, *21* (18), 13973-13996. DOI: https://doi.org/10.5194/acp-21-13973-2021.
(82) Peng, X.; Wang, T.; Wang, W.; Ravishankara, A. R.; George, C.; Xia, M.; Cai, M.; Li, Q.; Salvador, C. M.; Lau, C.; et al. Photodissociation of particulate nitrate as a source of daytime tropospheric Cl_2. *Nat. Commun.* **2022**, *13* (1), 939. DOI: https://doi.org/10.1038/s41467-022-28383-9.
(83) USGS. *US Geological Survey Mineral Commodity Summaries 2021*; Reston, VA, 2021. http://pubs.er.usgs.gov/publication/mcs2022 (accessed 2022-11-28). DOI: https://doi.org/10.3133/mcs2022.
(84) Toba, A.-L.; Nguyen, R. T.; Cole, C.; Neupane, G.; Paranthaman, M. P. U.S. lithium resources from geothermal and extraction feasibility. *Resources, Conservation and Recycling* **2021**, *169*, 105514. DOI: https://doi.org/10.1016/j.resconrec.2021.105514.
(85) Platt, U.; Stutz, J. Differential Optical Absorption Spectroscopy: Principles and Applications. Springer Verlag, 2008; pp 412 - 417.